Preparation of Biopex®-supported gold nanoparticles as a potential fiducial marker for image-guided radiation therapy

Kai Ikeda,[‡,a] Haoran Liu,[‡,a] Naoki Miyamoto,[b,c] Mai Thanh Nguyen,[a] Hiroki Shirato,[d] Tetsu Yonezawa[,a]*

[a]Division of Materials Science and Engineering, Faculty of Engineering, Hokkaido University, Kita 13 Nishi 8, Kita-ku, Sapporo, Hokkaido 060-8628, Japan

[b]Division of Applied Quantum Science and Engineering, Faculty of Engineering, Hokkaido University, Kita 13 Nishi 8, Kita-ku, Sapporo, Hokkaido 060-8628, Japan

[c]Department of Medical Physics, Hokkaido University Hospital, Kita 14 Nishi 5, Kita-ku, Sapporo, Hokkaido 060-8648, Japan

[d]Global Station of Quantum Medical Science and Engineering, Global Institution for Collaborative Research and Education, Hokkaido University, Kita 15 Nishi 7, Kita-ku, Sapporo, Hokkaido 060-8638, Japan

KEYWORDS: gold nanoparticle, apatite, calcium phosphate, bone cement, injectable, fiducial marker, image-guided radiation therapy

ABSTRACT: Image-guided radiation therapy (IGRT) has emerged as a promising technique for cancer treatment to improve radiation precision and accuracy, thereby reducing the treatment toxicity and optimizing therapeutic efficacy. In IGRT, fiducial markers are required to be inserted near the tumor to get the spatial information of the tumor. Currently used metal fiducial markers with large sizes would be highly invasive, it is therefore critical to develop minimally invasive alternatives to these markers. In this work, an injectable marker based on Biopex®-supported Au NPs with adequate radio-opacity for X-ray visualization was developed. Biopex can function as substrate for the growth of Au NPs and avoid excessive reaction-induced aggregation and precipitation. The self-curing property of Biopex prevents the leakage and elimination of isolated Au NPs, enabling long-term X-ray observation and radiotherapy. The effect of Biopex amount, gold precursor concentration, and reaction time were evaluated. The visibility of samples prepared by the optimized formula was also examined. The developed Biopex-Au NPs could be injected through a 21G needle and exhibit great visibility in X-ray visualization test, showing great potential as a fiducial marker for image-guided radiation therapy.

1. INTRODUCTION

Radiation therapy is one of the most used cancer treatments that uses beams of intense energy, such as X-rays and protons, to kill cancer cells by destroying their genetic material.[1,2] However, tumors rarely display a fixed position during irradiation due to breathing motion, peristalsis, and other body motions.[3,4] To compensate for variations in tumor position, image-guided radiation therapy (IGRT) has been commonly used in the clinic to improve radiation precision and accuracy, thereby reducing the treatment toxicity and optimizing therapeutic efficacy.[5,6] In IGRT, fiducial markers are required to be inserted near the tumor, then the computer could get the spatial information between the tumor and the fiducial marker by taking images of the diseased area. Normally, fiducial markers are metal-based solid implants with large physical dimensions.[5,7,8] These large-sized fiducial markers are considered highly invasive, especially for the elderly, and require complicated insertion procedures which might result in the risk of complications, such as pneumothorax,[9-11] infection,[12,13] and bleeding. It is therefore critical to explore minimally invasive alternatives to current large-sized tissue markers, such as injectable fiducial markers (colloidal- or liquid-like)[14-17] and several commercial markers, including Gold Anchor ™ Fiducial Markers, PolyMark ™ Fiducial Markers, BioXmark®.

Gold induces a strong X-ray attenuation owing to their higher atomic number and electron density than those of the currently used markers.[18] Besides, gold nanoparticles (Au NPs) have excellent biocompatibility, and ultra-small size, which make them an ideal candidate as long-term fiducial markers for radiotherapy through a minimally invasive way like injection.[19-21] Of all the methods for preparing Au NPs, the chemical reduction is the most used strategy in which gold ions in the precursor are reduced by reducing agents such as β-d-glucose,[22] glycerol,[23] and sodium citrate.[24] On the other hand, stabilizing agents such as surfactants,

polymers, and ligands. For example, oleyl amine, poly(vinyl alcohol) (PVA), poly(vinyl pyrrolidone) (PVP) as well as thiol molecules are used to prevent aggregation and flocculation of Au NPs in liquid.[25] Byproducts might be generated during reactions due to the introduction of reducing and stabilizing agents. These agents may induce biological toxicity, washing and water treatment are therefore indispensable.[26-28] Besides, the isolated Au NPs would be eliminated from the body through a combination of renal and hepatobiliary pathways[29]. Consequently, a green preparation of Au NPs and the following approach to deliver and fix Au NPs at the target sites are highly desired.

Biopex is a commercially available calcium phosphate cement that consists of powder and liquid phases. The powder phase is a mixture of α-tricalcium phosphate (α-$Ca_3(PO_4)_2$), tetracalcium phosphate ($Ca_4(PO_4)_2O$), dicalcium phosphate dihydrate ($CaHPO_4.2H_2O$), and hydroxyapatite ($Ca_{10}(PO_4)_6$ $(OH)_2$), whereas the liquid phase is an aqueous solution of a chondroitin sulfate sodium salt and succinic acid disodium salt as shown in **Table 1**.[30] Biopex has been wildly used for bone tissue repair because of its non-invasive injection, slight foreign-material reactions, rapid curing reaction. In this work, an injectable marker based on Biopex-supported Au NPs (Biopex-Au NPs) with adequate radio-opacity for X-ray visualization is developed, as illustrated in **Figure 1**. The powder phase was firstly mixed with gold precursor and reducing agent. Gold ions were reduced to form Au NPs on the surface of the powder, which avoids the aggregation between Au NPs and the extra use of stabilizing agents. The reducing agent, ethanol in this system, could be easily removed via centrifugation and vacuum drying. After mixing with the liquid phase, the paste could be injected through 18G, 19G, and 21G needles, and then self-cured at the injection site. This allows the minimally invasive injection of the fiducial marker and prevents the elimination of isolated Au NPs by the human body for long-

term X-ray observation and radiotherapy. The effect of Biopex amount, gold precursor concentration, and reaction time were evaluated. The visibility of samples prepared by the optimized formula was also examined. The developed Biopex-Au NPs fulfills the requirements of fiducial marker for IGRT as it is minimally invasive, remains in a solid and stable state after injection, and exhibits great visibility.

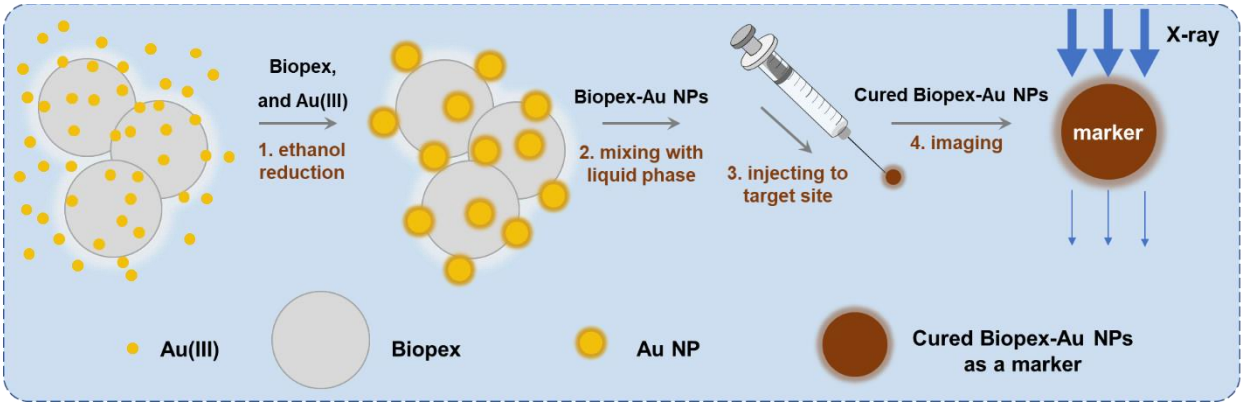

Figure 1. Schematic illustration of injectable Biopex-Au NPs for image-guided radiation therapy.

Table 1. Composition of the powder and liquid phases of Biopex

	Chemicals	Formular	Contents *
Powder phase	α-tricalcium phosphate	α-$Ca_3(PO_4)_2$	7.50 g
	tetracalcium phosphate	$Ca_4(PO_4)_2O$	1.80 g
	dicalcium phosphate dihydrate	$CaHPO_4.2H_2O$	0.50 g
	hydroxyapatite	$Ca_{10}(PO_4)_6(OH)_2$	0.20 g
Liquid phase	chondroitin sulfate sodium salt	-	54.05 mg
	succinic acid disodium salt	$(CH_2COONa)_2$	129.72 mg

* Contents in 10-g of powder and 1-mL of liquid

2. MATERIALS AND METHODS

2.1. Materials. Tetrachloroauric (Ⅲ) acid hydrate ($HAuCl_4$•nH_2O, n = 3.7, Kojima, Japan), Biopex (HOYA Technosurgical, Japan), and ethanol (Japan Alcohol Trading Co., Ltd., Japan) were used as a precursor, an additive, and reducing agent, respectively. 1g $HAuCl_4$•nH_2O (n = 3.7) was dissolved in 100 mL pure water to obtain a 24.6 mmol/L aqueous solution of $HAuCl_4$. Injection tests were carried out using 1-mL plastic syringes with the diameter of 4.2 mm and the length of 104 mm. All chemicals were used as received. Pure water was prepared using ELGA/Organo Purelab system (>18.2 MΩ·cm).

2.2. Preparation of Biopex-Au NPs. The fabrication route of Biopex-Au NPs is illustrated in **Figure S1**. Water, ethanol, and Biopex powder phase were mixed into a 2 L two-necked flask and was heated in an oil bath with heating temperature at 120 °C. 24.6 mM aqueous solution of $HAuCl_4$ was added when the mixed solution boiled. The final concentration of $HAuCl_4$ was

adjusted to 0.50, 0.75, 1.00 mmol/L. The concentration of ethanol was 50 v/v % and the amounts of Biopex were 99, 150, 160, 200, 257 mg. The reaction lasted for 2, 4, 6 hours with a condenser and stirring speed at 700 rpm. When the reaction is finished, the mixed solution was centrifugated for 10 minutes after a 10-minute ultrasonic process. The precipitate was collected and dried in a vacuum oven for 5 hours to obtain Biopex-Au NPs.

2.3. Characterization. UV-Vis spectra were collected to observe Au NPs formation by using a UV-Vis spectrophotometer (Shimadzu UV-1800) and a quartz cell with a 1-cm optical path. Transmission electron microscopy (TEM, JEOL JEM 2000-FX, at 200 kV) was used to analyze the morphology, size of Biopex-Au NPs. For TEM sample preparation, Au NPs dispersion was dropped on collodion film-coated copper TEM grids and left for natural drying. The phase composition of Biopex-Au NPs was examined by wide-angle X-ray diffraction (XRD, MiniFlex II, Rigaku). The morphologies of surfaces were observed using a field emission scanning electron microscope (FE-SEM, JSM-6701F, JEOL). The elemental analysis was evaluated by an X-ray fluorescence spectrometer (XRF, JSX-6710F, JEOL).

2.4. X-ray visualization tests. To evaluate the X-ray visualization of Biopex-Au NPs, the X-ray visualization test was conducted at the Central Institute of Isotope Science, Hokkaido University. **Figure S2** shows the schematic diagram of the X-ray visualization test. The samples and gold markers were irradiated with X-rays generated from an X-ray tube (UD-150-B40, Shimadzu Corporation), and the X-rays passed through the samples would be detected by the Flat Panel Detector (PaxScan 3030, Varian Medical System). Besides, acrylic resins that have an X-ray attenuation property close to the human body were placed between samples and the detector,[31] and the visualization ability was evaluated by the pattern matching scores quantified by the

detector. The pattern matching scores were calculated by the correlation coefficient according to a previous study.[32,33]

3. RESULTS AND DISCUSSION

3.1 Effect of Biopex on the prepared Au NPs. Firstly, the effect of Biopex on the prepared Au NPs was investigated with or without the addition of Biopex (99 mg), in which the $HAuCl_4$ concentration was 0.50 mmol/L and reaction time was 2 h. **Figure S3** shows the color change of the mixed solution with Biopex during the reaction. **Figure S4** shows the images of liquid samples with or without Biopex after synthesis and the dried Biopex-Au NPs. The liquid sample with Biopex appears dark red because the surface plasmon resonance (SPR) phenomenon causes absorption of light in the blue-green portion of the spectrum while the red light is reflected. **Figure 2 (a)** shows the UV-Vis spectra of Au NPs and Biopex-Au NPs. The spectrum of Au NPs exhibits an SPR peak with maximum absorption wavelength (λ_{max}) at 575 nm and the λ_{max} of Biopex-Au NPs is at 571 nm, suggesting the formation of Au NPs. TEM images of Au NPs and Biopex-Au NPs, along with their size distributions are shown in **Figure 2 (b)** and **(c)**. Most of the Au NPs are spherical with their average size of 211 ± 101 nm. In contrast, the average size of Biopex-AuNPs support is 107 ± 39 nm. Ethanol is a mild reducing agent, and hence, a relatively long reaction time is required for the formation of Au NPs. As a result of long reaction process and the lack of capping agent, the formed Au NPs assembled and merged. Instead, with the addition of Biopex, Au NPs would generate on the surface of Biopex, which reduces the possibility of contacting, assembling, and merging between Au NPs. Therefore, the average size of Au NPs on Biopex is smaller than that in pure ethanol. In general, the SPR absorption wavelength of NPs is size-dependent and larger NPs show longer λ_{max}.[34] Therefore, λ_{max} of the Au NPs and Biopex-Au NPs are longer than 510-520 nm which is typical λ_{max} range of Au NPs

with smaller sizes (10-30 nm). It is speculated that the Au NPs grew around the surface of Biopex powder appear like a weak aggregation state, causing a red shift in the λ_{max}. In addition, from both TEM and SEM images of Biopex-Au NPs (**Figure 2 (d)**), triangular and hexagonal Au NPs are also observed, which is corresponding to the SPR peak at around 740 nm and 850 nm in UV-Vis spectra. When reductions occur on the surface of Au nucleated seeds, they are dependent on the surface energy of the different crystal facets. Therefore, polygonal particles are generated. To further confirm the mass ratio of Biopex to Au NPs after the reaction, XRF analysis was conducted to quantitatively evaluate the elemental composition of samples. **Figure 2 (e)** shows the XRF result of Biopex-Au NPs. The quantitative values of P, Ca, and Au are 17.5 mol%, 56 mol%, and 26.5 mol%. O and H in Biopex have low atomic weights and were not detected by XRF analysis. Therefore, the mass ratio of gold and Biopex in Biopex-Au NPs was calculated based on the XRF and the following formula:

$$\frac{W_{Biopxe}}{W_{Au}} = \frac{\frac{5.0M_P}{N_{Ca}}N_P + (5.0M_{Ca} + 13.0M_O + 0.2M_H)N_{Ca}}{5.0M_{Au}N_{Au}} = \frac{154.80N_P + 408.62N_{Ca}}{985.00N_{Au}}$$

in which M_P, M_{Ca}, M_O, M_H, and M_{Au} are the atomic weight of P, Ca, O, H, and Au, and N_P, N_{Ca}, and N_{Au} are the quantitative values (mol %) of P, Ca, and Au from the XRF result. From Table 1, the molar ratio of each element in Biopex is P: Ca: O: H = 3.0: 5.0: 13.0: 0.2. The mass ratio of Biopex to Au NPs was 0.98: 1.00 after calculation, whereas the theoretical mass ratio is 2.00: 1.00, implying that about half of Biopex was lost during the preparation of Biopex-Au NPs.

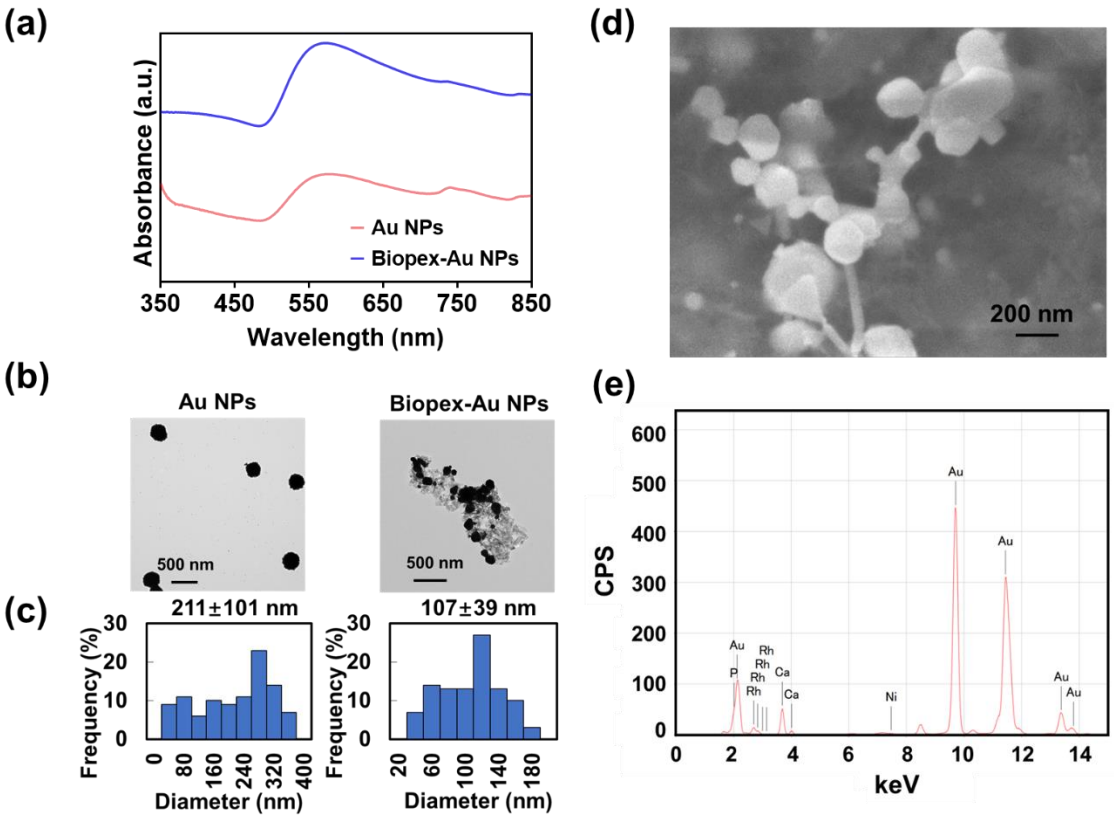

Figure 2. (a) UV-Vis spectra of Au NPs and Biopex-Au NPs prepared by ethanol reduction. (b) TEM images and (c) particle size distributions of Au NPs and Biopex-Au NPs. (d) SEM image of Biopex-Au NPs. (e) XRF of Biopex-Au NPs.

3.2. Effect of Biopex amounts on Biopex-Au NPs and changes of Biopex during the reaction.

In this section, the effect of Biopex amounts (99, 150, 160, 200, 257 mg) on the prepared Au NPs was investigated. **Figure 3 (a)** shows the UV-Vis spectra of Biopex-Au NPs with different amounts of Biopex. The λ_{max} of the Biopex-Au NPs with Biopex amounts of 99, 150, 160, 200, and 257 mg are at 571, 574, 573, 583, and 579 nm, respectively. As shown in **Figure 3 (b)** and **(c)**, the TEM images show the morphologies of Au NPs supported with different amounts of Biopex and their average sizes are 107±39, 104±35, 111±57, 102±32, and 107±42 nm. As the results of the growth of Au NPs on Biopex substrates, these Biopex-Au NPs appear in "weak

aggregations" states. The Biopex amount had no notable effect on the size of Au NPs and the states of weak aggregation of Au NPs. Therefore, negligible shift of λ_{max} was observed. The mass ratio of each sample ware calculated and shown in **Figure 3 (d)**. There is a linear relationship between the mass ratio of Biopex to Au NPs and the amount of Biopex used for supporting Au NPs. It also reveals that a certain and similar amount of Biopex (about 60 to 70 mg) would be lost during the reaction even the amounts of added Biopex for supporting Au NPs were different (from 99 to 257 mg). To track the loss of Biopex during the reaction, the supernatant after centrifugation was collected by an evaporator and then dried by a vacuum oven. **Figure S5** shows the collected white powders, and the elemental composition was evaluated by XRF. As shown in **Figure 3 (e)**, in addition to Ca and P derived from Biopex, Cl derived from $HAuCl_4$ was also detected. To further investigate the changes of Biopex during the reaction, XRD of Biopex, Biopex-Au NPs, and the white powder collected from the supernatant were measured and the result are shown in **Figures 4** and **5**. The spectra of the components in Biopex, $Ca_3(PO_4)_2$, $Ca_4(PO_4)_2O$, $CaHPO_4$, and $Ca_{10}(PO_4)_6$, are also shown as references. From the spectrum of Biopex-Au NPs, the diffraction peaks of gold could be observed, confirming the composite structure of Biopex-supported Au NPs. Differences in the characteristic peaks at 2θ of 30-35° reveal that the original $Ca_3(PO_4)_2$ and $Ca_4(PO_4)_2O$ diminished gradually as a result of the reaction between $Ca_3(PO_4)_2$, $Ca_4(PO_4)_2O$ and HCl, which was generated with the reduction of gold. The formation of $CaClH_2PO_4.H_2O$ was confirmed by the XRD of the white powder collected from the supernatant. Therefore, it is considered that part of Biopex would react with HCl and form $CaClH_2PO_4$ during the reaction, while Au^{3+} would be reduced and grow on the remaining Biopex.

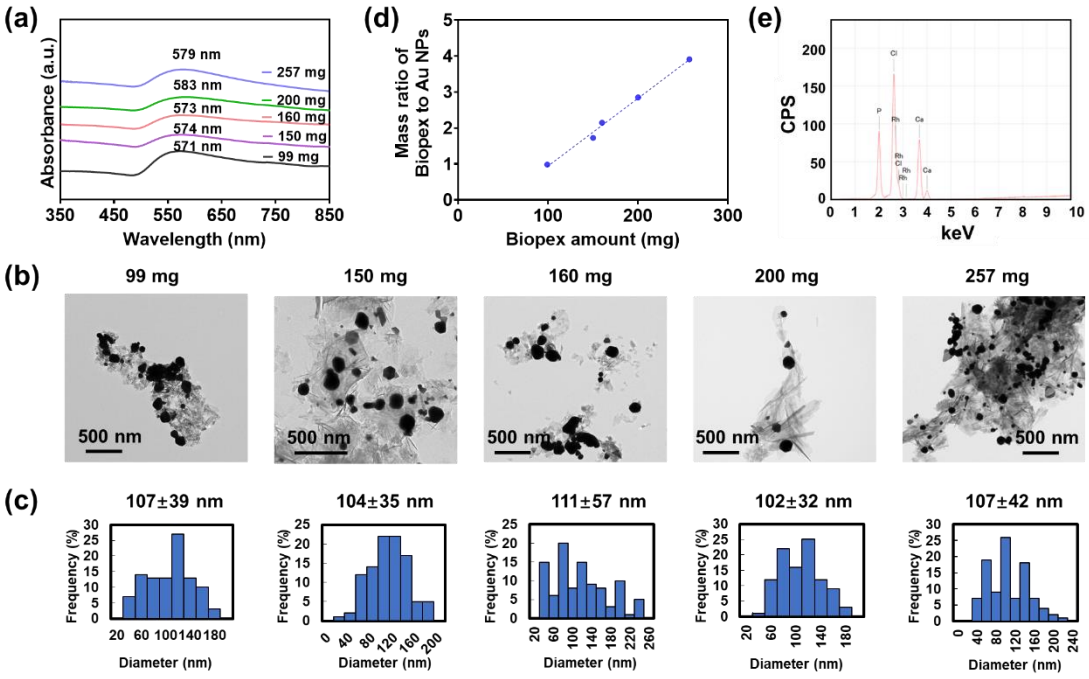

Figure 3. (a) UV-Vis spectra of Biopex-Au NPs prepared with different Biopex amounts. (b) TEM images and (c) particle size distributions of Biopex-Au NPs prepared with different amounts of Biopex. (d) The mass ratio of Biopex to Au NPs of Biopex-Au NPs prepared with different Biopex amounts. (e) XRF of white powder collected from the supernatant.

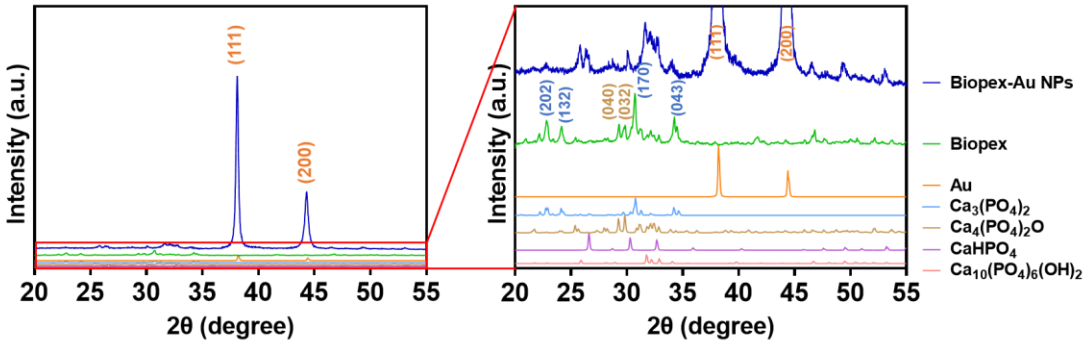

Figure 4. XRD of Biopex-Au NPs and Biopex. XRD peak index of Au, $Ca_3(PO_4)_2$, and $Ca_4(PO_4)_2O$ are written in orange, blue, and green, respectively.

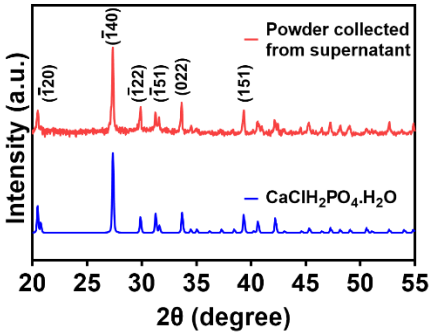

Figure 5. XRD of white powder collected from the supernatant.

3.3. Effect of $HAuCl_4$ concentration on Biopex-Au NPs. Figure 6 (a) shows the UV-Vis spectra of Biopex-Au NPs prepared with different concentrations of $HAuCl_4$. The λ_{max} of Biopex-Au NPs prepared with $HAuCl_4$ concentrations of 0.50, 0.75, and 1.00 mmol/L are at 571 nm, 583 nm, and 593 nm, respectively. As shown in **Figure 6 (b)** and **(c)**, the morphology of Au NPs is not significantly affected by the varied $HAuCl_4$ concentrations, but the average particle sizes of the Au NPs are 107±39, 145±61, and 157±77 nm when the concentrations of $HAuCl_4$ are 0.50, 0.75 and 1.00 mmol/L, respectively. The average particle sizes of Au NPs increase with the increasing concentration of $HAuCl_4$ and the larger particles sizes cause the red shift of λ_{max} from 571 to 593 nm. Weak aggregation states of Au NPs on Biopex seems to have less impact on the λ_{max} than the particle size of Biopex-Au NPs when varying the concentration of $HAuCl_4$. The particle size distributions also become broad when $HAuCl_4$ concentrations increase. During the preparation process, a higher concentration of $HAuCl_4$ would increase the possibility and frequency of gold nucleation. The increasing gold nuclei would tend to agglomerate during the reaction, resulting in larger average particle size and broad particle size distribution.

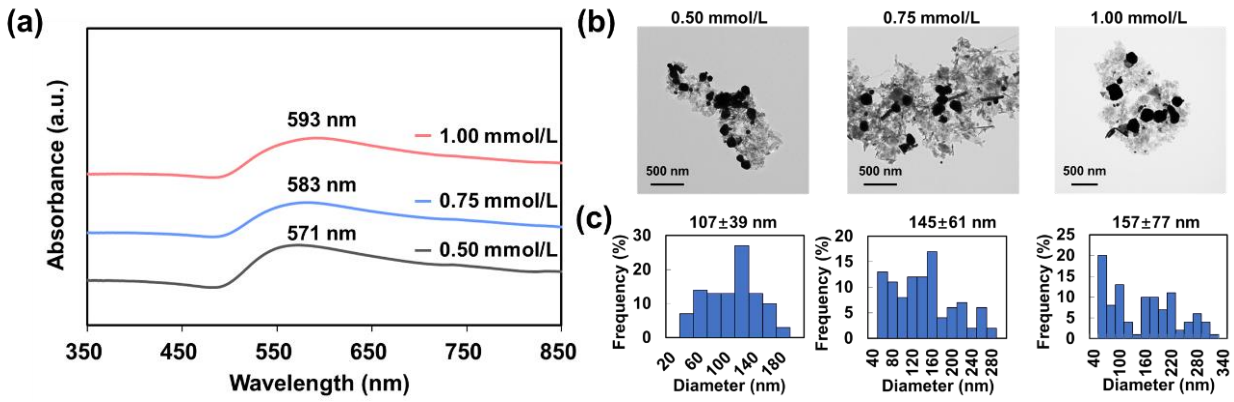

Figure 6. (a) UV-Vis spectra of Biopex-Au NPs prepared with different $HAuCl_4$ concentrations. (b) TEM images and (c) particle size distribution of Biopex-Au NPs prepared with different $HAuCl_4$ concentrations.

3.4. Effect of reaction time on Biopex-Au NPs. In this section, the effect of reaction time (2, 4, and 6 hours) on the Biopex-Au NPs was investigated. **Figure 7 (a)** shows the UV-Vis spectra of the Biopex-Au NPs with different reaction times. The λ_{max} of the Biopex-Au NPs with a reaction time of 2, 4, and 6 hours are at 593, 592, and 594 nm, respectively. The insignificant differences in the λ_{max} of Au NPs with different reaction times suggest that reaction time had a minor effect on the yield of Au NPs. It is also consistent with the size of the Au NPs as shown in the TEM images. **Figure 7 (b)** and **(c)** shows the TEM images and the particle size distributions of the samples with different reaction times. It can be noted that the different reaction times have a negligible effect on the morphology as well as the average size of the Au NPs, though the deviations in the particle size distribution can still be observed.

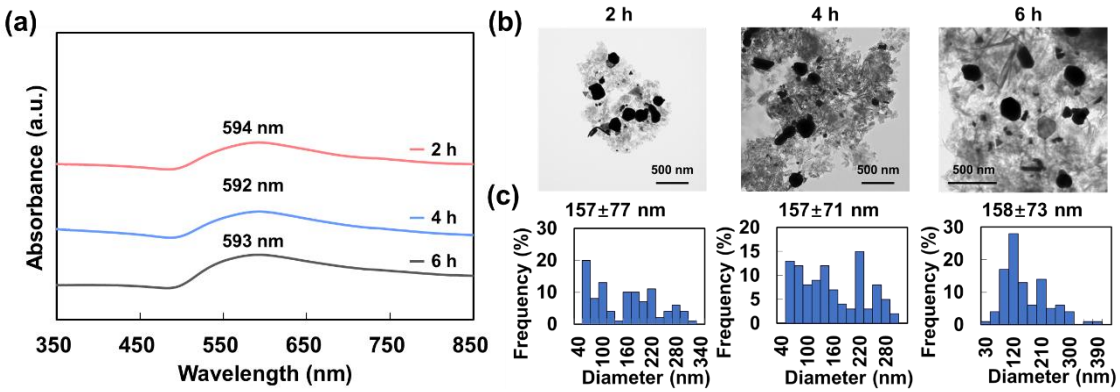

Figure 7. (a) UV-Vis spectra of Biopex-Au NPs with different reaction times of 2, 4, and 6 hours. (b) TEM images and (c) particle size distribution of Biopex-Au NPs prepared with different reaction times.

3.5. Injection and X-ray visualization ability of Biopex-Au NPs. In previous sections, the effect of Biopex amount, $HAuCl_4$ concentration, and reaction time on the Biopex-Au NPs were investigated. Considering the comprehensive properties of Biopex-Au NPs, the optimized reaction conditions were determined for the following injection and X-ray visualization test, in which the concentration of $HAuCl_4$ was 1.00 mmol/L, the mass ratio of Biopex to Au NPs was 2:1, and the reaction time was 4 hours. To compensate for the loss of Biopex during the reaction, extra Biopex was added to ensure the mass ratio of Biopex to Au NPs is 2:1 for balancing the X-ray imaging efficiency and the strength of Biopex-Au NPs after injection. 1.5 g Biopex-Au NPs was mixed with 0.4 mL liquid phase in a mixing syringe (Togo Medikit, Japan) and the paste was transferred into an injection syringe (Togo Medikit, Japan). The Biopex-Au NPs paste was then injected into jelly through 18G (outer diameter 1.25 ± 0.02 mm, inner diameter 0.82 ± 0.03 mm), 19 G (outer diameter 1.08 ± 0.02 mm, inner diameter 0.69 ± 0.03 mm), and 21 G (outer diameter 0.81 ± 0.02 mm, inner diameter 0.51 ± 0.03 mm) needles to assess the injection ability and the shape-retaining ability after injection. **Figure S6** shows the Biopex-Au NPs injected

through 18G, 19G, and 21G needles. Since the needle with an inner diameter of 2 mm is required for a 1.5-mm gold marker, Biopex-Au NPs is considered minimally invasive as it could be injected by a 21G needle. As shown in **Figure S7**, Biopex-Au NPs were collected from jelly 30 mins after the injection, exhibiting a self-curing performance and excellent shape-retaining ability.

Figure 8 (a) shows images obtained from an X-ray visualization test. **Table 2** and **Figure 8 (b)** show the results of the pattern matching score calculated based on the X-ray visualization images. A pattern matching score is regarded as a quantitative measurement of the visibility of an object in relation to its surroundings. The pattern matching score ranging from 1 to 1oo is calculated by the correlation coefficient. When the pattern matching score is over 30, it indicates that the marker could be recognized correctly by the detector with high tracking accuracy and is considered to have sufficient visibility for motion tracking during IGRT. As shown in **Figure 8 (b)**, when the resin thickness is 5 cm, the visibility of pure Biopex is lower than that of other samples, and the samples injected through 18G and 19G have similar visibility with gold markers. The pattern matching score decreased with increasing acrylic resin thickness, suggesting the human body also causes the attenuation of X-ray. The higher the pattern matching score under thicker acrylic resin indicates that the marker would have better imaging performance deep inside the human body. When the acrylic resin increased to 15 cm, pure Biopex becomes hard to identify, while Biopex-Au NPs are still highly visible. Biopex-Au NPs could even be recognized under 20-cm acrylic resin and 160-mA tube current. Compared to the gold markers, the visibility of Biopex-Au NPs is slightly inferior to the 2.0-mm gold marker but shows better imaging ability than the 1.5-mm gold marker. Notably, the Biopex-Au NPs injected through a 21G needle is less visible than the other samples due to the less amount of gold caused

by accidental crack. In comparison with some fiducial markers based on Au NPs, the Biopex could support the growth of Au NPs and then act as delivery agent to deliver Au NPs at desired site around tumor.[35,36] The rapid curing nature of Biopex also enables long-term fixation of Au NPs *in vivo* and renders Biopex-Au NPs a longer life span than iodine-based fiducial markers.[17] Accordingly, Biopex-Au NPs are considered sufficient for IGRT.

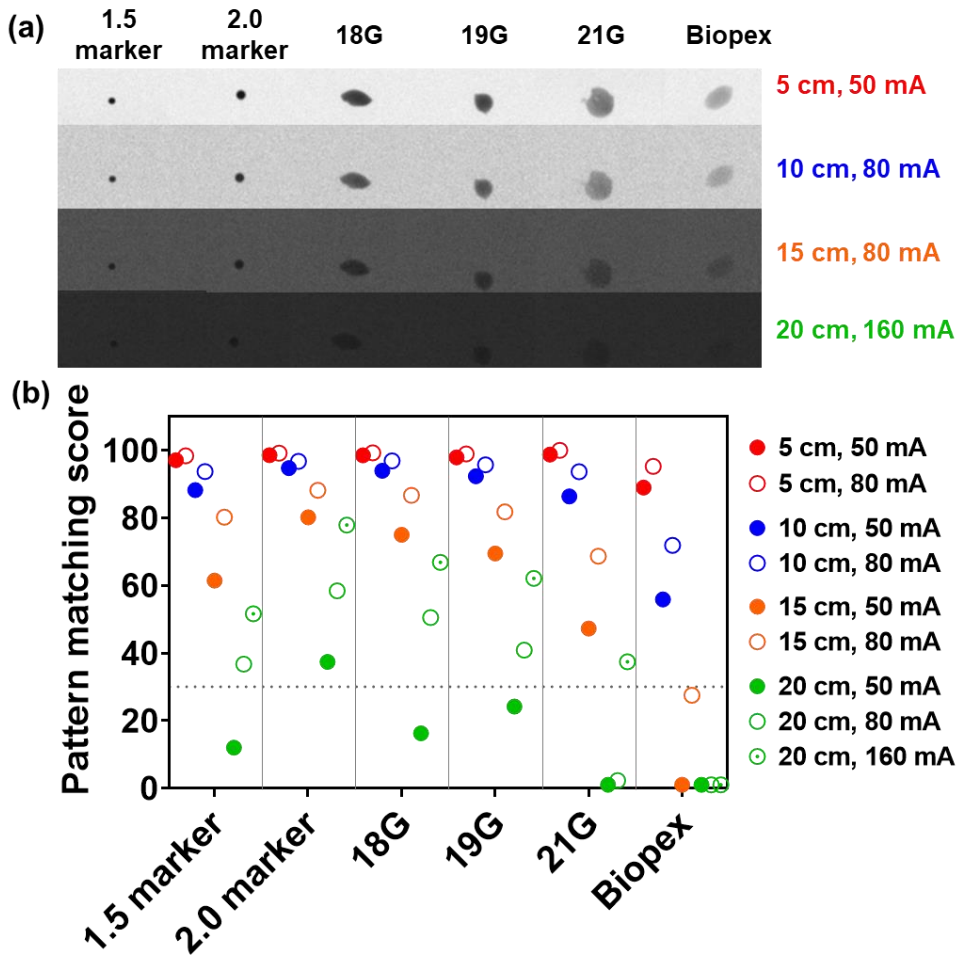

Figure 8. (a) X-ray visualization images and (b) pattern matching scores of 1.5-mm gold marker, 2.0-mm gold marker, Biopex-Au NPs injected through 18G, 19G, 21G needles, pure Biopex under different acrylic resin thickness and tube currents with a constant X-ray tube voltage of 110 kV.

Table 2. Visibility evaluation based on pattern matching scores

Acrylic resin thickness (cm)	Tube current (mA)	1.5-mm gold marker	2.0-mm gold marker	18G Biopex-Au NPs	19G Biopex-Au NPs	21G Biopex-Au NPs	Biopex
5	50	97.08	98.58	98.51	97.9	98.77	88.96
5	80	98.39	99.15	99.27	98.93	100	95.27
10	50	88.25	94.75	93.97	92.31	86.37	55.87
10	80	93.72	96.75	96.89	95.72	93.68	71.88
15	50	61.43	80.17	75.00	69.48	47.24	1.00
15	80	80.24	88.19	86.7	81.79	68.67	27.50
20	50	12.00	37.39	16.24	24.16	1.00	1.00
20	80	36.74	58.43	50.49	40.88	2.28	1.00
20	160	51.61	77.88	66.87	62.08	37.4	1.00

4. CONCLUSIONS

In this work, an injectable marker based on Biopex-supported Au NPs was fabricated via a green synthesis by using ethanol as a reducing agent. Biopex helped (1) mediate the growth of Au NPs and prevent their assembly and merging, (2) transfer Au NPs to target site via thin needles, (3) prevent the elimination of Au NPs by the human body, and (4) complement the imaging function of Au NPs. The effects of Biopex amount, gold precursor concentration, and reaction time on Biopex-Au NPs were evaluated. The optimized conditions are determined in which the concentration of $HAuCl_4$ was 1.0 mmol/L, the mass ratio of Biopex to Au NPs was 2:1, and the reaction time was 4 hours. The injection ability and visibility of Biopex-Au NPs prepared by the

optimized formula were also examined. The developed Biopex-Au NPs could be injected through a 21G needle (outer diameter 0.81 ± 0.02 mm, inner diameter 0.51 ± 0.03 mm) and exhibit great visibility in the X-ray visualization test. Biopex-Au NPs are therefore considered fulfilling the requirements of fiducial marker for IGRT. Although Biopex-Au NPs has shown potential as a fiducial marker, more efforts and studies should be made in follow-up work, including cytotoxicity, long-term toxicity, animal test, and potential side effect.

Corresponding Author

* Tetsu Yonezawa. E-mail address: tetsu@eng.hokudai.ac.jp.

Author Contributions

K.I. performed the experiments, collected and analyzed data. H.L. assisted the experiments, analyzed data, and wrote the manuscript. N.M. performed X-ray visualization test and analyzed data. M.T.N. helped the analysis with constructive discussions. H.S. and T.Y. conceived the idea. T.Y. directed and supervised the research. The manuscript was written through contributions of all authors. All authors have given approval to the final version of the manuscript. ‡These authors contributed equally.

Notes

The authors declare no competing financial interest.

Supporting Information. Supporting information file includes: Fabrication route of Biopex-Au NPs; Schematic diagram of the X-ray visualization test; Color change of the mixed solution in the synthesis experiment with $HAuCl_4$ concentration 0.50 mmol/L, reaction time 2 hours, Biopex amount 99 mg; Optical images of liquid samples with and without Biopex after 2-hour synthesis

and the dried Biopex-Au NPs; White powder collected from the supernatant; Biopex-Au NPs injected through 18G, 19G, and 21G needles; Cured Biopex-Au NPs taken out from jelly.

ACKNOWLEDGMENTS

This work was partially supported by Hokkaido University. This work is also supported in part by The Translational Research program; Strategic PRomotion for practical application of INnovative medical Technology (TR-SPRINT) funded by The Japan Agency for Medical Research and Development (AMED), by Grants-in-Aid for Regional R&D Proposal-Based Program from Northern Advancement Center for Science & Technology (NOASTEC) of Hokkaido Japan and by JKA Foundation (Promotion fund from KEIRIN RACE: 2021-M113). Authors thank Dr. Y. Ishida and Mr. H. Tsukamoto (Hokkaido University) for fruitful discussions and experimental assistance. Authors also gratefully acknowledge Hokkaido University Hospital Clinical Research and Medical Innovation Centre for the fruitful discussions and the technical assistances. We gratefully acknowledge the Central Institute of Isotope Science (CIS), Hokkaido University for assistance for X-ray visualization test. The authors thank Mr. T. Tanioka, and Ms. R. Yokohira (Hokkaido University) for their assistance in TEM-EDS analysis. H.L. would like to thank the China Scholarship Council (CSC) for the financial support of his work in Sapporo, Japan.

REFERENCES

(1) Baskar, R.; Lee, K. A.; Yeo, R.; Yeoh, K. W. Cancer and radiation therapy: current advances and future directions. *Int. J. Med. Sci.* **2012**, *9* (3), 193.

(2) Yan, D.; Vicini, F.; Wong, J.; Martinez, A. Adaptive radiation therapy. *Phys. Med. Biol.* **1997**, *42* (1), 123.

(3) Jølck, R. I.; Rydhög, J. S.; Christensen, A. N.; Hansen, A. E.; Bruun, L. M.; Schaarup-Jensen, H.; von Wenck, A. S.; Børresen, B.; Kristensen, A. T.; Clausen, M. H. Injectable colloidal gold for use in intrafractional 2D image-guided radiation therapy. *Adv. Healthc. Mater.* **2015**, *4* (6), 856-863.

(4) Giraud, P.; Yorke, E.; Jiang, S.; Simon, L.; Rosenzweig, K.; Mageras, G. Reduction of organ motion effects in IMRT and conformal 3D radiation delivery by using gating and tracking techniques. *Cancer Radiother.* **2006**, *10* (5), 269-282.

(5) Arosio, P.; Avolio, M.; Gargano, M.; Orsini, F.; Gallo, S.; Melada, J.; Bonizzoni, L.; Ludwig, N.; Veronese, I. Magnetic stimulation of gold fiducial markers used in Image-Guided Radiation Therapy: Evidences of hyperthermia effects. *Measurement* **2020**, *151*, 107242.

(6) Fischer-Valuck, B. W.; Henke, L.; Green, O.; Kashani, R.; Acharya, S.; Bradley, J. D.; Robinson, C. G.; Thomas, M.; Zoberi, I.; Thorstad, W. Two-and-a-half-year clinical experience with the world's first magnetic resonance image guided radiation therapy system. *Adv. Radiat. Oncol.* **2017**, *2* (3), 485-493.

(7) Park, W. G.; Yan, B. M.; Schellenberg, D.; Kim, J.; Chang, D. T.; Koong, A.; Patalano, C.; Van Dam, J. EUS-guided gold fiducial insertion for image-guided radiation therapy of pancreatic cancer: 50 successful cases without fluoroscopy. *Gastrointest. Endosc.* **2010**, *71* (3), 513-518.

(8) Lehmann, J.; Perks, J.; Semon, S.; Harse, R.; Purdy, J. A. Commissioning experience with cone-beam computed tomography for image-guided radiation therapy. *J. Appl. Clin. Med. Phys.* **2007**, *8* (3), 21-36.

(9) Machiels, M.; van Hooft, J.; Jin, P.; van Berge Henegouwen, M. I.; van Laarhoven, H. M.; Alderliesten, T.; Hulshof, M. C. Endoscopy/EUS-guided fiducial marker placement in patients with esophageal cancer: a comparative analysis of 3 types of markers. *Gastrointest. Endosc.* **2015**, *82* (4), 641-649.

(10) Bhagat, N.; Fidelman, N.; Durack, J. C.; Collins, J.; Gordon, R. L.; LaBerge, J. M.; Kerlan, R. K. Complications associated with the percutaneous insertion of fiducial markers in the thorax. *CardioVasc. Interv. Radiol.* **2010**, *33* (6), 1186-1191.

(11) Kothary, N.; Heit, J. J.; Louie, J. D.; Kuo, W. T.; Loo Jr, B. W.; Koong, A.; Chang, D. T.; Hovsepian, D.; Sze, D. Y.; Hofmann, L. V. Safety and efficacy of percutaneous fiducial

marker implantation for image-guided radiation therapy. *J. Vasc. Interv. Radiol.* **2009**, *20* (2), 235-239.

(12) Loh, J.; Baker, K.; Sridharan, S.; Greer, P.; Wratten, C.; Capp, A.; Gallagher, S.; Martin, J. Infections after fiducial marker implantation for prostate radiotherapy: are we underestimating the risks? *J. Radiat. Oncol.* **2015**, *10* (1), 1-5.

(13) Fawaz, Z.; Yassa, M.; Nguyen, D.; Vavassis, P. Fiducial marker implantation in prostate radiation therapy: complication rates and technique. *Cancer Radiother.* **2014**, *18* (8), 736-739.

(14) de Souza Lawrence, L.; Ford, E.; Gilbert, C.; Yarmus, L.; Meneshian, A.; Feller-Kopman, D.; Hales, R. Novel applications of an injectable radiopaque hydrogel tissue marker for management of thoracic malignancies. *Chest* **2013**, *143* (6), 1635-1641.

(15) Ahn, S. H.; Gil, M. S.; Lee, D. S.; Han, Y.; Park, H. C.; Sohn, J. W.; Kim, H. Y.; Shin, E. H.; Yu, J. I.; Noh, J. M. Preclinical investigation for developing injectable fiducial markers using a mixture of $BaSO_4$ and biodegradable polymer for proton therapy. *Med. Phys.* **2015**, *42* (5), 2626-2637.

(16) Shin, K.; Choi, J. W.; Ko, G.; Baik, S.; Kim, D.; Park, O. K.; Lee, K.; Cho, H. R.; Han, S. I.; Lee, S. H. Multifunctional nanoparticles as a tissue adhesive and an injectable marker for image-guided procedures. *Nat. Commun.* **2017**, *8* (1), 1-12.

(17) Schaarup-Jensen, H.; Jensen, A. I.; Hansen, A. E.; El Ali, H. H.; Hammershøj, P.; Jølck, R. I.; Kjær, A.; Andresen, T. L.; Clausen, M. H. Injectable iodine-125 labeled tissue marker for radioactive localization of non-palpable breast lesions. *Acta Biomater.* **2018**, *65*, 197-202.

(18) Popovtzer, R.; Agrawal, A.; Kotov, N. A.; Popovtzer, A.; Balter, J.; Carey, T. E.; Kopelman, R. Targeted gold nanoparticles enable molecular CT imaging of cancer. *Nano Lett.* **2008**, *8* (12), 4593-4596.

(19) Dong, Y. C.; Hajfathalian, M.; Maidment, P. S.; Hsu, J. C.; Naha, P. C.; Si-Mohamed, S.; Breuilly, M.; Kim, J.; Chhour, P.; Douek, P. Effect of gold nanoparticle size on their properties as contrast agents for computed tomography. *Sci. Rep.* **2019**, *9* (1), 1-13.

(20) Zhang, L.; Yang, X.; Wei, J.; Li, X.; Wang, H.; Zhao, Y. Intelligent gold nanostars for in vivo CT imaging and catalase-enhanced synergistic photodynamic & photothermal tumor therapy. *Theranostics* **2019**, *9* (19), 5424.

(21) Cormode, D. P.; Roessl, E.; Thran, A.; Skajaa, T.; Gordon, R. E.; Schlomka, J.-P.; Fuster, V.; Fisher, E. A.; Mulder, W. J.; Proksa, R. Atherosclerotic plaque composition: analysis with multicolor CT and targeted gold nanoparticles. *Radiology* **2010**, *256* (3), 774-782.

(22) Huang, H.; Yang, X. Synthesis of polysaccharide-stabilized gold and silver nanoparticles: a green method. *Carbohydr. Res.* **2004**, *339* (15), 2627-2631.

(23) Parveen, R.; Ullah, S.; Sgarbi, R.; Tremiliosi-Filho, G. One-pot ligand-free synthesis of gold nanoparticles: the role of glycerol as reducing-cum-stabilizing agent. *Colloids Surf., A Physicochem. Eng. Asp.* **2019**, *565*, 162-171.

(24) He, Y. Q.; Liu, S. P.; Kong, L.; Liu, Z. F. A study on the sizes and concentrations of gold nanoparticles by spectra of absorption, resonance Rayleigh scattering and resonance non-linear scattering. *Spectrochim. Acta A Mol. Biomol. Spectrosc.* **2005**, *61* (13-14), 2861-2866.

(25) Nishimoto, M.; Yonezawa, T.; Čempel, D.; Nguyen, M. T.; Ishida, Y.; Tsukamoto, H. Effect of H_2O_2 on Au nanoparticle preparation using microwave-induced plasma in liquid. *Mater. Chem. Phys.* **2017**, *193*, 7-12.

(26) Liu, S.; Han, M. Synthesis, functionalization, and bioconjugation of monodisperse, Silica-Coated gold nanoparticles: Robust bioprobes. *Adv. Funct. Mater.* **2005**, *15* (6), 961-967.

(27) Brust, M.; Fink, J.; Bethell, D.; Schiffrin, D.; Kiely, C. Synthesis and reactions of functionalised gold nanoparticles. *J. Chem. Soc., Chem. Commun.* **1995**, (16), 1655-1656.

(28) Vijayan, S. R.; Santhiyagu, P.; Singamuthu, M.; Kumari Ahila, N.; Jayaraman, R.; Ethiraj, K. Synthesis and characterization of silver and gold nanoparticles using aqueous extract of seaweed, Turbinaria conoides, and their antimicrofouling activity. *Sci. World J.* **2014**, *2014*, 938272.

(29) Poon, W.; Zhang, Y.-N.; Ouyang, B.; Kingston, B. R.; Wu, J. L.; Wilhelm, S.; Chan, W. C. Elimination pathways of nanoparticles. *ACS Nano* **2019**, *13* (5), 5785-5798.

(30) Tanaka, S.; Kishi, T.; Shimogoryo, R.; Matsuya, S.; Ishikawa, K. Biopex® acquires anti-washout properties by adding sodium alginate into its liquid phase. *Dent. Mater. J.* **2003**, *22* (3), 301-312.

(31) Caldas, M. d. P.; Ramos-Perez, F. M. d. M.; Almeida, S. M. d.; Haiter-Neto, F. Comparative evaluation among different materials to replace soft tissue in oral radiology studies. *J. Appl. Oral Sci.* **2010**, *18* (3), 264-267.

(32) Miyamoto, N.; Ishikawa, M.; Bengua, G.; Sutherland, K.; Suzuki, R.; Kimura, S.; Shimizu, S.; Onimaru, R.; Shirato, H. Optimization of fluoroscopy parameters using pattern matching prediction in the real-time tumor-tracking radiotherapy system. *Phys. Med. Biol.* **2011**, *56* (15), 4803.

(33) Hamada, T.; Sutherland, K.; Ishikawa, M.; Miyamoto, N.; Honma, S.; Shirato, H.; Honma, K. In vivo imaging of clock gene expression in multiple tissues of freely moving mice. *Nat. Commun.* **2016**, *7* (1), 1-13.

(34) Suchomel, P.; Kvitek, L.; Prucek, R.; Panacek, A.; Halder, A.; Vajda, S.; Zboril, R. Simple size-controlled synthesis of Au nanoparticles and their size-dependent catalytic activity. *Sci. Rep.* **2018**, *8* (1), 1-11.

(35) Wang, Z.; Wu, L.; Cai, W. Size-tunable synthesis of monodisperse water-soluble gold nanoparticles with high X-ray attenuation. *Eur. J. Chem.* **2010**, *16* (5), 1459-1463.

(36) Xu, C.; Tung, G. A.; Sun, S. Size and concentration effect of gold nanoparticles on X-ray attenuation as measured on computed tomography. *Chem. Mater.* **2008**, *20* (13), 4167-4169.

SYNOPSIS

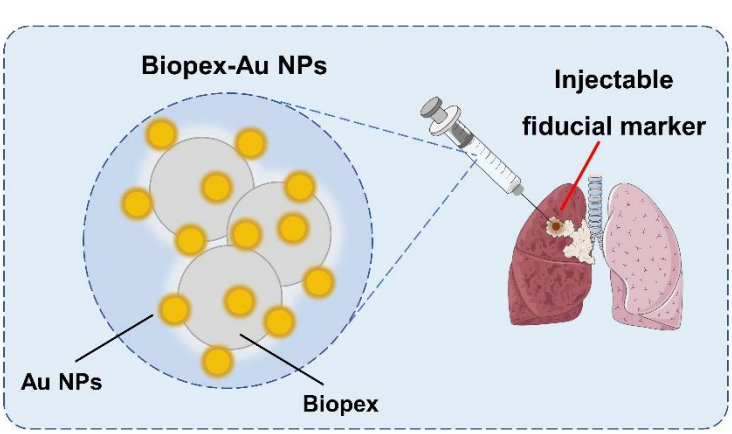
Biopex-Au NPs
Injectable
fiducial marker
Au NPs
Biopex

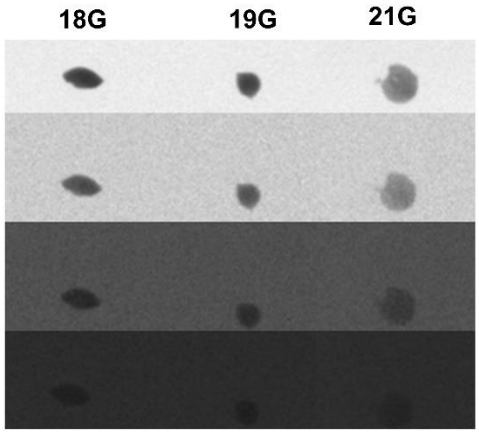
18G
19G
21G